NEW APPROACHES FOR ANALYSIS OF JET NOISE DATA

N. Karthikeyan* and L. Venkatakrishnan**

Abstract

Despite the significant advances in Computational Aeroacoustics for predicting jet noise, there is still a considerable need for experimental data. However, traditional measures of the directivity of Overall Sound Pressure Levels or the spectral distribution of the acoustic energy yield limited understanding of the nature of the sources. There is hence a need to use different approaches to the analysis of jet acoustics, among them applications of statistical methods such as auto correlation, self-correlation etc to understand the noise sources. In this paper, the acoustic characteristics of supersonic and high subsonic jets from nozzles of different exit geometries are measured and analyzed using these methods. The results show that these statistical methods of analysis can reveal the presence of two distinct noise sources in the flow and are applicable to both subsonic and supersonic flows. The information can be used to determine the appropriate model for the data and is useful for forming new theories about the noise generation mechanism in turbulent jets.

Introduction

The noise from the jet engine exhaust is one of the major components of aircraft noise. The problem of supersonic jet noise has been investigated very extensively since the 50s [1]. However, a complete description that explains all observed phenomena is lacking, as is universal agreement on a theory of noise generation in turbulent, often heated flows. Such a theory is urgently needed for developing a suitable suppression technique. The suppression of jet noise is of paramount importance, both from the view of the increasingly stringent criteria for commercial aircraft as well as the needs of stealth for military aircraft. Over the past several decades, significant progress has been made towards theoretical descriptions of jet noise [2-4]; its experimental documentation [5-8] and on its numerical prediction using large-eddy simulation (LES) and direct numerical simulation (DNS). Previous studies [9] have shown that a two-pronged strategy of experimental and computational approaches is best suited to handle such jet flows.

The need to identify the noise generation mechanisms and relate changes in the flow to the acoustic field in order to evolve methods of suppression has led to a enormous effort in experimental aeroacoustics [10-19]. It is now well accepted that jet noise can be thought of as having three components namely the screech caused by supersonically convecting large structures [20]; broadband shock associated noise caused by the passage of these structures through the shock cells and turbulent mixing noise which occurs in both high subsonic and supersonic jets. The last is the most difficult to suppress as the sources of mixing noise are not clearly understood.

The mixing noise is directionally independent and consists of higher frequencies. This sound is generated in the same manner as in subsonic flow by the fine-scale chaotic turbulence. Analysis of experimental data by Tam [21] clearly shows the contributions of the distinct components to the total far-field spectrum: the Mach wave radiation due to large-scale motions and radiation due to small-scale turbulence. Tam [22] has suggested a "Two-Source Model", according to which the sources of jet noise radiated in the downstream and sideline directions are physically different; the sound generated by large scale structures is highly coherent and is highly dominant in the downstream direction while small scale structures contribute to noise in all directions incoherently.

The identification of these two distinct sources is extremely difficult with traditional non-simultaneous single or multiple microphones. Typical setup scenarios involved measurements with microphones mounted along a polar array or a linear array with the microphones arranged at regular intervals. These studies have been carried out in both acoustic near field and far field, with supersonic and subsonic nozzles of different exit geometry. The acoustic

* Scientist **Head
Experimental Aerodynamics Division, Council of Scientific and Industrial Research (CSIR), National Aerospace Laboratories, Post Box No. 1779, Kodihalli, Bangalore-560 017, India, Email : venkat@nal.res.in

field of the jet emanating from the nozzles is usually characterized by analysis of the frequency spectra obtained from the microphone signals. Further, these studies were limited to comparisons between sound pressure levels and OASPLs alone or correlations between two microphones traversed along the jet flow direction [19,22]. The comparisons were able to provide a qualitative view of advantage or disadvantage of a nozzle configuration but shed very little light on noise source modification due to nozzle exit geometry. It has been realized that the jet noise source identification efforts require simultaneous measurements that can be correlated to ascertain the extent of sources both in time and space.

Due to the lack of high speed instrumentation, earlier efforts at simultaneous measurements were limited to two or three microphones directed at regions of interest. Recently, high fidelity systems capable of multi-channel simultaneous data acquisition with sampling rates as high as 250 kHz have been developed. Such systems have expanded the horizons of jet noise research and provided the researchers with capabilities to apply different statistical tools such as cross-correlation factor, coherence, bi-coherence etc., other than just auto-correlation factor. These tools provide new methods for understanding jet noise localization and its characterization using far-field measurements. Nance [23] suggests using these tools to separate the contributions of small-scale and large-scale turbulence which has been successfully used to validate the "Two-source Noise model" in [24].

This paper presents a look at one such approach towards analyzing jet noise data. Statistical tools are used to compare the acoustic field of a supersonic flow through a C-D nozzle of design Mach number 1.5, operating at ideally expanded condition and high subsonic flow at a Mach number of 0.8 issuing through convergent nozzles of circular and rectangular exit geometries. Since turbulent mixing noise occurs in both high subsonic and supersonic jets, it is of interest to see whether there are similar features which can be extracted by the application of these statistical tools.

Experimental Setup

Facility

The measurements were carried out in the Jet Aeracoustics Research facility at NAL. The jet is supplied with dry compressed air from a 10 bar reservoir through a computerized globe valve (Make: Fisher, Type: ET). The driving pressure for the jet was maintained to within ±0.35 psi during the run. The jet exhausts in to an anechoic chamber (Fig.1a) of inner dimensions 3.6m (L) x 3.6m (W) x 3m (H) for carrying out acoustic measurements.

The anechoic chamber walls are mounted with fiberglass covered acoustic wedges, which are designed to achieve a low-frequency cutoff of 330 Hz. A catcher of 0.6m x 0.6m outlet provided with proper acoustic termination collects the jet exhaust. Preliminary acoustic tests showed that the room is anechoic above 400Hz with a partial floor grating in place. Fifteen microphones were set up in an arc that had a radial distance of 1.93m from the nozzle exit. This corresponded to 50.6 diameters for the C-D nozzle, 76 diameters for the circular convergent nozzle and 67.3 diameters for the convergent rectangular nozzle. As all three cases are sufficiently farther than the regulation 35 diameters distance, the measurements are thus in the acoustic far-field.

The arc (shown in Fig.1a) covered the polar angle, θ ranging from 90° to 160° (0° being jet inlet axis) with a spacing of 5°. The corrections for the actuator response as well as the free-field response are applied at each frequency. The corrected SPL values are then converted back into pressure values and integration is then performed over the corrected spectrum. The resulting squared pressure value is then used to obtain the OASPL.

Figures 1b and 1c present two views of the anechoic chamber showing the jet pipe with nozzle, microphone setup and the exit catcher.

Instrumentation

The acoustic measurements were carried out with 15, 1/4 in diameter B & K Type 4939 (TEDS enabled) Falcon® range free-field microphones. The data acquisition is carried out through B & K's Lan XI (11 x 3 channel 102.4 kHz module) simultaneous data acquisition system. The data was acquired using PULSE® Time Data Recorder module which is specifically designed for real-time data acquisition and analysis. The simultaneous measurements from all the 15 microphones were recorded and stored in ASCII text format. The signals from the microphones were sampled at the rate of 262 kHz thus providing usable data up to 100kHz. This has been established to be sufficient for studies on jet mixing noise. For each angular location, 409600 samples were collected and analyzed with a 4096 point fast Fourier transform (FFT) and averaged. Averaging the results for the 100 subsets reduced the

random error in the calculation to within 0.1%. The resulting resolution of the narrowband spectra is 48.8Hz. The sound pressure level (SPL) is defined in the conventional manner,

$$SPL = 20 \log_{10} \left(\frac{P_{rms}}{P_{ref}} \right) \quad (1)$$

where p_{ref} is taken as 20 μPa. The overall sound pressure level (OASPL) was calculated by numerical integration of the spectra.

Nozzle

Three types of nozzles were used in the present study - an axisymmetric convergent-divergent (C-D) nozzle with design Mach number of 1.5, and two subsonic convergent nozzles of which one had a circular and the second had a rectangular exit. The rectangular nozzle had a ratio of width to height of 4:1. The exit areas of the nozzles are 1.767 in^2, 0.7853 m^2 and 1 m^2 respectively. These sonic nozzles are manufactured using fiber reinforced plastics (FRP) while supersonic nozzle is fabricated using SS-304. For the FRP nozzles, the nozzle lip thickness is maintained at 2mm keeping in mind the limitations on the strength of the FRP at small thicknesses. For the CD nozzle the nozzle lip thickness is 0.5mm. The rectangular nozzle has a h/d ratio of 4:1. Table-1 gives a summary of the nozzle geometry.

The nozzles were fitted to the jet pipe by using an adapter. The nozzles were designed such that whatever be the geometry, the exit of the nozzle was always coincided with the center of the microphone arc. The nozzles are shown in Fig.1d. The rectangular nozzle can be operated in two configurations. These correspond to the longer side being horizontal or vertical. This is achieved by an azimuthal rotation of the nozzle, designated by the angle ϕ which corresponds to 0° for the horizontal (longer side) case and 90° for the vertical case.

Table-1 : Summary of Nozzle Geometry

Nozzle		Diameter (in)	Area ($inch^2$)	Area (m^2)
Converging-Diverging		1.5	1.76625	0.01139514
Converging	Circular	1	0.785	0.000506451
	Rectangular	1 (w) x 0.25 (h) AR 4:1, Eqvt. Dia. = 1.129	1	0.00064516

Test Conditions

In the present study, the nozzles are run ideally expanded at a pressure ratio such as to result in an exit Mach number of 1.5 as in case of the C-D nozzle and a subsonic Mach number of 0.8 for the convergent nozzles. This was achieved by setting different nozzle pressure ratios (NPR) is defined as stagnation pressure (P_o) to the ambient static pressure (P_a). For the Mach 1.5 nozzle, ideal expansion at the nozzle exit is obtained at NPR of 3.66, while the ideal NPR for sonic nozzles is 1.89. For the chosen subsonic Mach number of 0.8, this corresponded to an NPR of 1.52. Ambient pressure and temperature in the anechoic room are measured at 13.27psi (P_a) and 293 K (T_a), respectively.

Analysis

The purpose of this analysis is to determine whether the time series of the acoustic signals of mixing noise displays the behavior of a random process or there is an underlying order within in. The presence of such order can be used to determine the appropriate model for the data. While there are a number of statistical methods available, both simple and complicated, some of them are very specific for certain purposes.

This section presents the statistical tools which were used to analyze the time-series data obtained from the microphone signals. Three tools namely, autocorrelation, cross correlation and coherence are presented.

Autocorrelation

Auto correlation or self correlation is the measure of how well a signal remembers itself in time. It represents the coherence of the signal in time. For the given signal from the n^{th} microphone $p_n(t)$ with a time delay of τ seconds, the normalized auto correlation function is given by,

$$R_{n\,n}(\tau) = \frac{| p_n(t) \bullet p_n(t+\tau) |}{| p_n^2(t) |} \quad (2)$$

Here, |.|, indicate the ensemble or the time averaged values of the signal, and R_{nn} is the autocorrelation coefficient. For a completely random signal the values of autocorrelation are very low or zero.

Cross-correlation

Cross correlation between two time signals measures how well the signals correspond together. The time signals have to be acquired simultaneously. If R_{mn} is large and positive, it means that an increase in the first signal corresponds with increase in the other and vice versa. On the other hand if is large and negative, then increase in the first signal corresponds with decrease in the other. A cross correlation factor very low and near to zero indicate that the two signals dont correspond at all. For better understanding the cross correlation factor is generally normalized with the magnitude of the signals so that the values remain between -1 and 1.

Cross correlation between two microphone signals m and n is defined by,

$$R_{m\,n}(\tau) = \frac{|\, p_m(t) \bullet p_n(t+\tau)\,|}{\sqrt{|\, p_m^2(t)\,|}\ \sqrt{|\, p_n^2(t)\,|}} \qquad (3)$$

Here, |.|, indicate the ensemble or the time averaged values of the signal and R_{nm} is the autocorrelation coefficient.

Coherence Function

The coherence function is the measure of linear dependency between two signals as the function of the frequency. It is a function of frequency. This implies that it enables us to ascertain the correlation at each frequency i.e., correlations that exist between the spectral components. The coherence function C_{mn} between two microphone signals m and n is given by,

$$\gamma_{mn}^2(f) = \frac{|\, G_{mn}(f)\,|^2}{G_{mm}(f)\, G_{nn}(f)} \qquad (4)$$

Where, $G_{mn}(f)$ is the cross power spectrum between the two microphone signals, $G_{mm}(f)$ and $G_{nn}(f)$ are the auto power spectrum of the m^{th} and n^{th} microphone signal respectively.

Results and Discussions

The comparison of overall sound pressure level for nozzle for different nozzle exit configurations is shown in Fig.2. The noise level from the supersonic nozzle is considerably greater than that of the subsonic nozzles as expected as known from the work of Lighthill [2,3] who showed that the acoustic power increased as the cube of the exit velocity. Further, the noise distribution from the supersonic nozzle exhibits the signature directivity pattern characteristic of supersonic jets with the convection and Mach wave radiation effects adding up towards the peak. This is because turbulent structures responsible for noise generation start to convect at supersonic speeds relative to the surrounding flow giving rise to Mach wave radiations. This component of noise which radiates predominantly in the downstream direction increases noticeably after an angle of 130° and peaks at an angle of 150°. Fig.3 shows the sound pressure level plots for microphone locations from 90° to 160°, at a distance of about 1.93m from the nozzle exit plane. The location legend is provided in Fig.3a. It is observed there is increase in noise levels at lower frequencies particularly in the downstream direction for all the nozzles. This increase in SPL for supersonic flow is very much higher than for the subsonic particularly in the downstream direction, hence the directivity pattern. It is seen that it is difficult to obtain any more insight into noise fields with only SPL and OASPL comparisons.

Normalized auto correlations at selected microphone locations, over a period of 2ms, are presented in Fig.4a-d. The autocorrelations for all locations are not shown here in order to reduce clutter. The time delay τ is about 300ms corresponding to the sampling frequency of 262 kHz. The numbers of samples taken for a correlation is 262 samples or for a time period of 1ms. These sub-plots show the normalized autocorrelation values for the nozzles operating at conditions described above. A detailed look at the plots reveals that, for all configurations, certain consistent trends and features are observed in the normalized autocorrelation values. Autocorrelations of microphone data at location angles lower than $\theta = 130°$ show a more spiky signal spread over a smaller time interval (τ), than at angles greater than 130° which is the angle of Mach wave radiation. At all angles the values of self-correlations at $\tau = 0$ ms is unity as expected. For $\theta < 130°$ the value of normalized autocorrelation drops to low values within very small τ as one would expect from small scale turbulence being completely random. Further, on careful examination the normalized auto correlation values for 120°

show a narrow spike with superposed skirts of lesser correlation at rather longer durations of τ. Tam [24] attributes this to the presence of two different timescales associated with small scale turbulence: one due to the small scale turbulence itself and other due to the modulation of noise from these structures which are being convected downstream by larger structures in the flow. The time over which these larger structures are correlated is much longer than that for small scale turbulence. This leads to autocorrelation shapes with the skirt. Beyond θ = 130°, the plot of autocorrelation coefficient exhibits a much wider base, without the presence of any skirt. This indicates that the correlation timescales at these angles is much larger and also that there are not multiple timescales associated with large scale turbulence. This leads us to conclude that there are two distinct sources of jet noise irrespective of the nozzle configuration. While the similarity of these plots for Mach numbers ranging from 0.3 to 0.9 was commented on in an earlier investigation [23], the current work which shows that this similarity extends even to the data for the supersonic case is revealing as to the nature of the noise generating mechanisms. The plots also show the presence of negative correlation peaks for the angles beyond 130°. These can be explained as resulting from the correlation between the compression and expansion regions in the acoustic waves.

Figures 5a-d presents the cross-correlations at eight locations which were the same as used for the autocorrelation, with the reference microphone at 120°, which is outside the Mach wave radiation region. It must be kept in mind that, for the location of 120°, this corresponds to a self-correlation. It is seen that the cross-correlation levels are very low with the neighboring microphones within the mach wave radiation cone. The cross-correlation of the reference with microphones above 120° shows even lower values. The maximum peak is around 0.3 for the rectangular convergent nozzle at 110°. Interestingly for the ideally expanded C-D nozzle case even such correlation peaks are not observed indicating there is no correlation at all at other locations.

Figures 6a-d presents the cross correlation data with reference microphone at 150° which is inside the cone of Mach wave radiation. Here a strong correlation with neighboring microphones within the mach wave radiation cone is observed. The value of the maximum cross-correlation falls as we proceed away from the reference microphone. There is very little or no correlation for θ = 130° which is outside the cone of Mach wave radiation.

Comparison of the results of the cross correlation with the reference microphone at 150° to those with the microphone at 120° leads us to conclude that the zone of significant spatial and temporal correlation is within the region of Mach wave radiation. This is the zone associated with high intensity and low frequency Mach waves.

Figures 7a-d presents the results of calculations of coherence of the spectra with the reference microphone at 120°. The plots are presented in a semilog format in order to improve their readability. The well known fact that jet noise coherence reduces with increased frequency is immediately seen in the plots. The plots help us to understand the how well correlated the signal is at a given frequency. As is expected, the coherence of the reference microphone with itself is unity.

The coherence between the microphones is found to fall to low levels beyond 10 kHz. Here again, the sound radiated is highly coherent within the mach wave radiation cone. Outside this region, the value of coherence is rather small and quickly reduces even for frequencies lower than 10 kHz.

Figures 8a-d presents the coherence calculated with the reference microphone at 150°. Again the coherence of the reference microphone with itself is unity. It is observed that the coherence of the neighboring microphones with the reference is much higher than seen in the previous figure for the reference at 120°. This is in line with the earlier finding of greater spatial and temporal coherence in the region of Mach wave radiation.

Figure 7c,d and Fig.8c,d show that for the far-field measurement there is no distinction between the orientation of the rectangular nozzle for the high and low angles. However the values for the intermediate angles between 120° to 150° show differences. This is in line with the OASPL plot presented earlier which showed similar trends.

Conclusions

Acoustic measurements were carried out on three nozzle configurations. Measurements were made with 15 microphones in an arc of constant radius in the far field. Data was taken for three conditions: one supersonic Mach number of 1.5 running at ideally expanded conditions and three subsonic Mach numbers of 0.8 with differing nozzle geometry. The results are analyzed using autocorrelation, cross correlation and coherence methods. The analysis

shows the presence of two distinct sources in jet noise, a fact that is not revealed by conventional methods of examining the directivity and spectral spread of the sound pressure levels. The methods help to discern order in such apparently random noise data which can be used to frame new theories about the mechanism of noise generation in turbulent jets.

Acknowledgments

The authors wish to thank Mr. Prashant Chougule for his help during the acoustic measurements.

References

1. Tam, C. K. W., "Jet Noise: Since 1952", Theoret. Comput. Fluid Dynamics, 10, pp.393-405, 1998.

2. Lighthill, M. J., "On Sound Generated Aerodynamically I. General Theory". Proc. R Soc. London, A 211, pp.564-587,1952.

3. Lighthill, M. J., "On Sound Generated Aerodynamically II. Turbulence as a Source of Sound". Proc. R. Soc. London, A 222, pp.1-32, 1954.

4. Lilley, G. M., "On the Noise from Jets", AGARD CP-131, 1974

5. Goldstein, M. E., "A Generalized Acoustic Analogy", J. Fluid Mech. 488, pp.315-333, J. Sound Vib., 50, pp.405-428, 2003.

6. Davies, P. O. A. L., Fisher, M. J. and Barratt, M. J., "The Characteristics of the Turbulence in the Mixing Region of a Round Jet", J. Fluid Mech., 15, pp.337-367, 1963.

7. Bradshaw, P., Ferriss, D. H. and Johnson, R. F., "Turbulence in the Noise Producing Region of a Circular Jet", J. Fluid Mech., 19, pp.591-624, 1964.

8. Tanna, H. K., "An experimental Study of Jet Noise Part II: Shock Associated Noise", J. Sound Vib., 50, pp.429-444, 1977.

9. Viswanathan, K., "Aeroacoustics of Hot Jets", J. Fluid Mech., 516, pp.39-82, 2004.

10. Viswanathan, K., Shur, M. L., Spalart, P. R. and Strelets, M. Kh., "Comparisons Between Experiment and Large-Eddy Simulation for Jet Noise", AIAA Journal, Vol. 45, No. 8, 2007.

11. Tam, C. K. W., "Supersonic Jet Noise, Annual Review of Fluid Mechanics, 27, pp.17-43, 1975.

12. Powell, A., "On the Mechanism of Choked Jet Noise", Proceedings of the Royal Society of London, 66 (408B), pp.1039-1056, 1953.

13. Raman, G., "Supersonic Jet Screech: Half-century from Powell to the Present", Journal of Sound and Vibration, 225 (3), pp.543-571, 1999.

14. Panda, J., "An Experimental Investigation of Screech Noise Generation", J. Fluid Mech., Vol.378, pp.71-96, 1999.

15. Shen, H. and Tam, C.K.W., "The Effects of Jet Temperature and Nozzle Lip Thickness on Screech Tones", AIAA Journal, Vol.38, No.5, pp.762-767, February 2000.

16. Norum, T.D., "Screech Suppression in Supersonic Jets", AIAA Journal, Vol.21, pp.235-240, February 1983.

17. Laufer, J,, Schlinker, R. and Kaplan, R.E., "Experiments on Supersonic Jet Noise", AIAA Journal, 14(4), pp.489-497, 1976.

18. Tam. C.K.W., Pastouchenko, N. and Schlinker, R.H., "On the Two Sources of Supersonic Jet Noise", AIAA 2003-3163, 9th AIAAJCEAS Aeroacoustics Conference and Exhibit (24th AJAA Aeroacoustics Conference), May 2003.

19. Hileman J. and Samimy, M., "An attempt to Identify Noise Generating Turbulent Structures in High Speed Axisymmetric Jet", AIAA-2000-2020, 6th AIAAJCEAS Aeroacoustics Conference and Exhibit (21st AJAA Aeroacoustics Conference), June 2000.

20. Tam, C.K.W., "Jet Noise: Since 1952", Theoretical and Computational Fluid Dynamics, 10(1-4), pp.393-405, January 1998.

21. Powell, A., "On the Mechanism of Choked Jet Noise", Proceedings of the Physical Society, B 66 (408). pp.1039-1056, R. Soc. London, A 211, pp.564 587, December 1953.

22. Tam, C.K.W., "Jet Noise Generated by Large-scale Coherent Motion", In Aeroacoustics of Flight Vehicles: Theory and Practice, Vol.1: Noise Sources (ed. H. H. Hubbard), pp.311-390, NASA RP-1258, WRDC TR-90-3052, 1991.

23. Nance, D.K., "Separating Contributions of Small-Scale Turbulence, Large-Scale Turbulence, and Core Noise from Far-Field Exhaust Noise Measurement", Ph.D. Thesis, Georgia Institute of Technology, 2007.

24. Tam, C.K.W., Vishwanathan, K., Ahuja, K. and Panda, J., "The Sources of Jet Noise: Experimental Evidence", AIAA 2007-3641, 13th AIAA/CEAS Aeroacoustics Conference, 28th AIAA Aeroacoustics Conference.

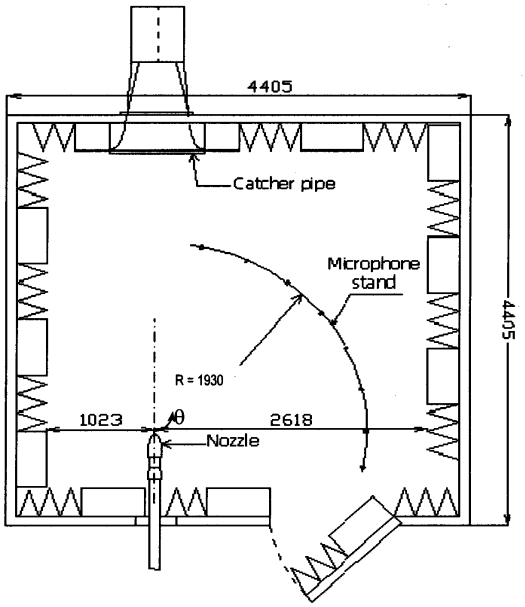

Fig.1a : Schematic Showing Anechoic Chamber and Microphone Placement (All dimensions in mm)

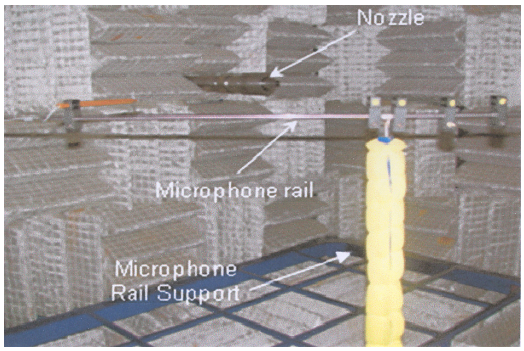

Fig.1b View of Anechoic Chamber Towards Inflow End

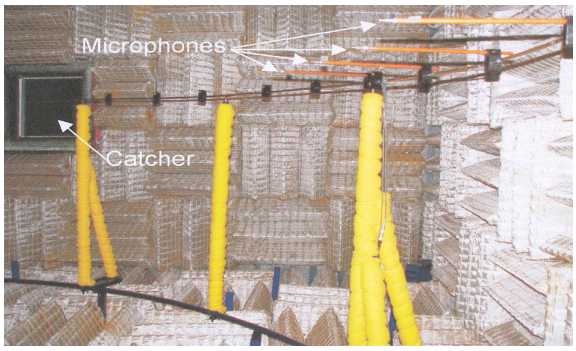

Fig.1c View of Anechoic Chamber Towards Catcher End

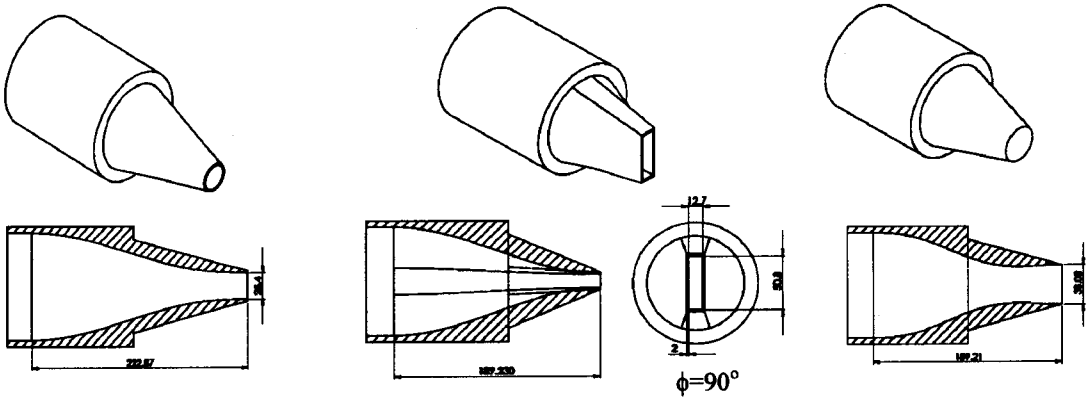

Fig.1d Nozzles used in Present Study

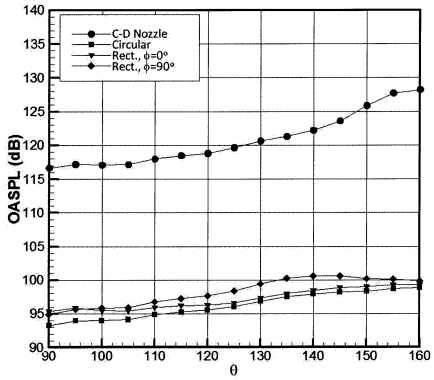

Fig.2 OASPL Comparison for Nozzles of Different Exit Geometries

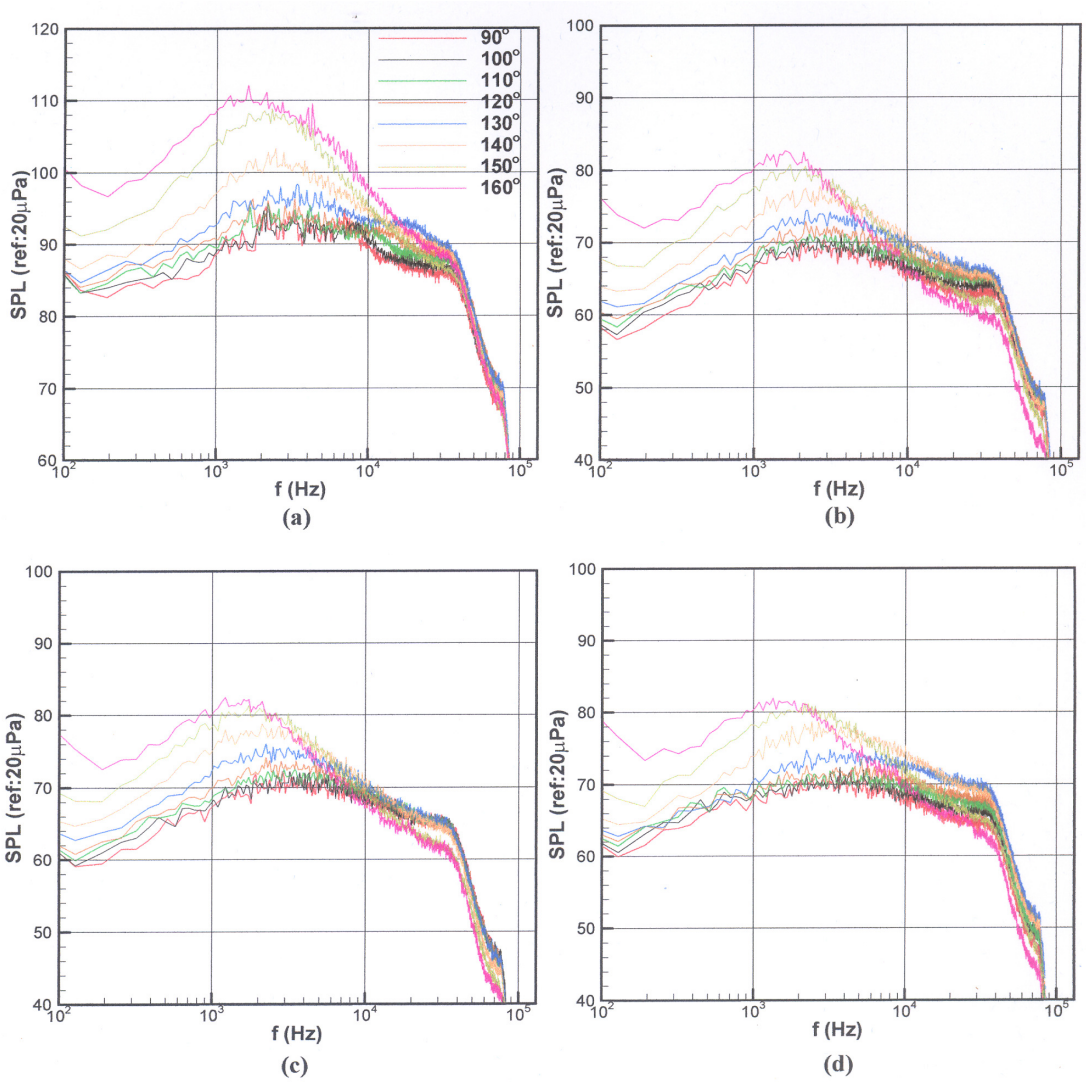

Fig.3 Variation of Sound Pressure Level with Frequency for the four Configurations (a) M=1.5, C-D Nozzle, (b) M=0.8, Circular Nozzle, (c) M=0.8 Rectangular (ϕ=0°), Convergent Nozzle, (d) M=0.8 Rectangular (ϕ=90°), Convergent Nozzle

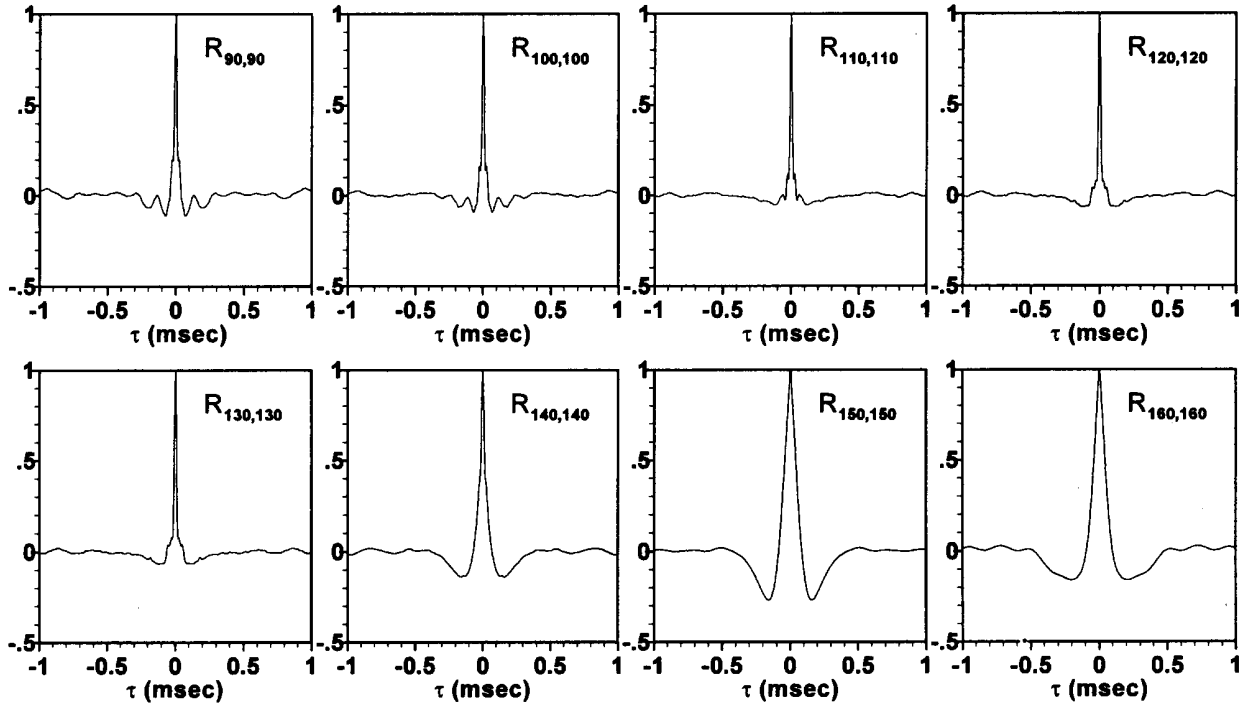

Fig.4 Auto-correlation for Microphones at all Locations (a) CD Nozzle M=1.5

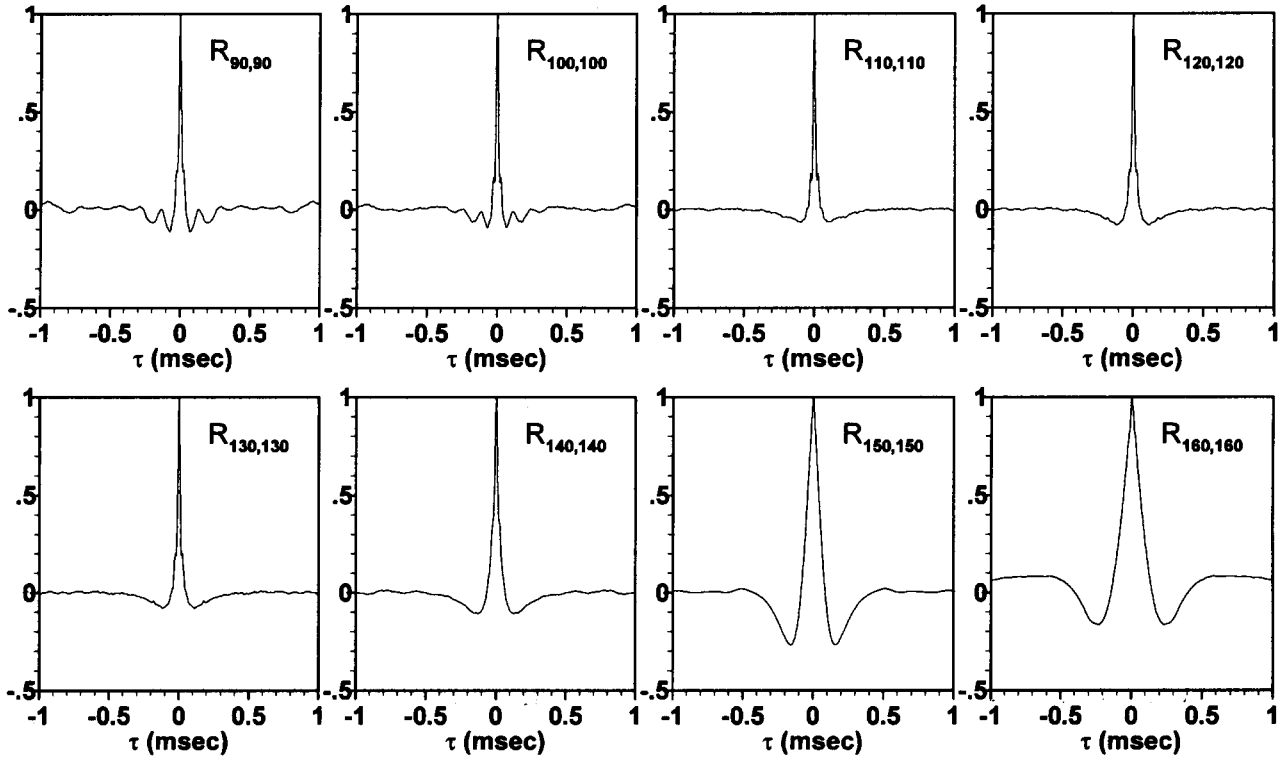

Fig.4 Auto-correlation for Microphones at all Locations (b) Circular Convergent Nozzle M=0.8

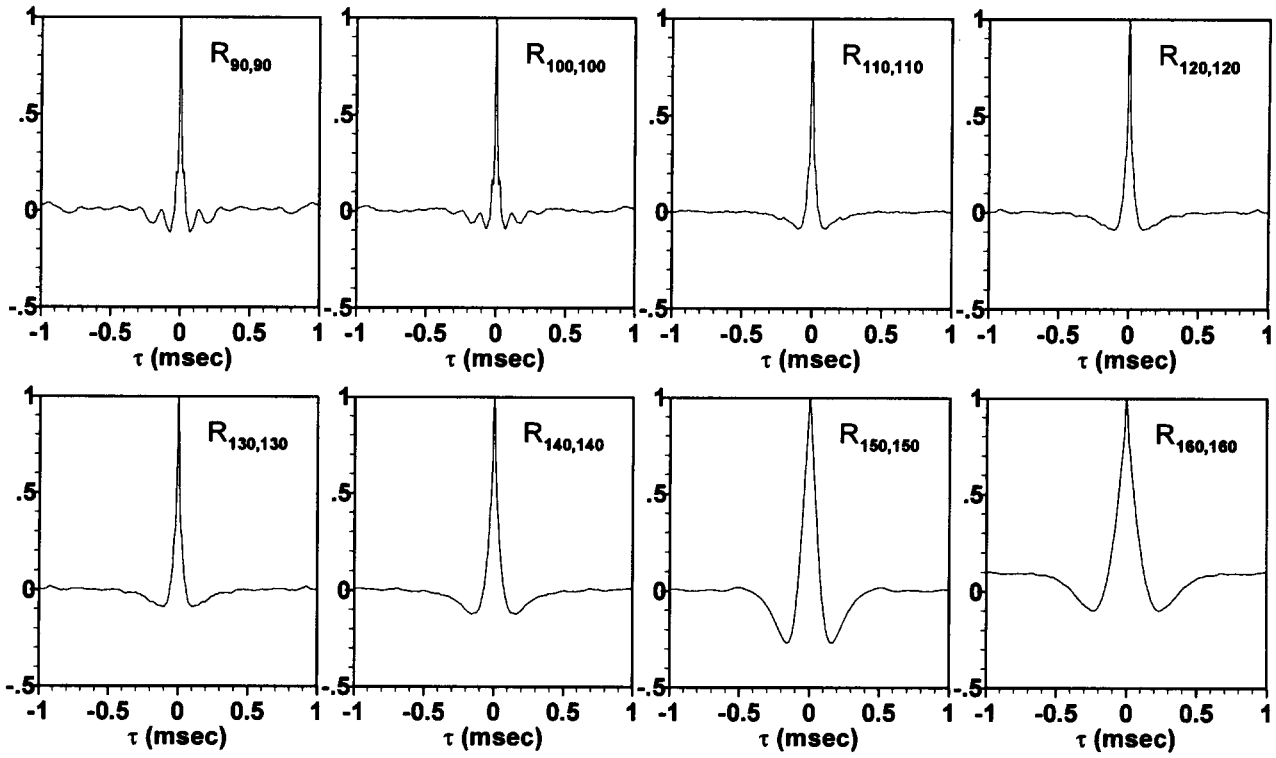

Fig.4 Auto-correlation for Microphones at all Locations (c) Rectangular Convergent Nozzle M=0.8, ϕ=0°

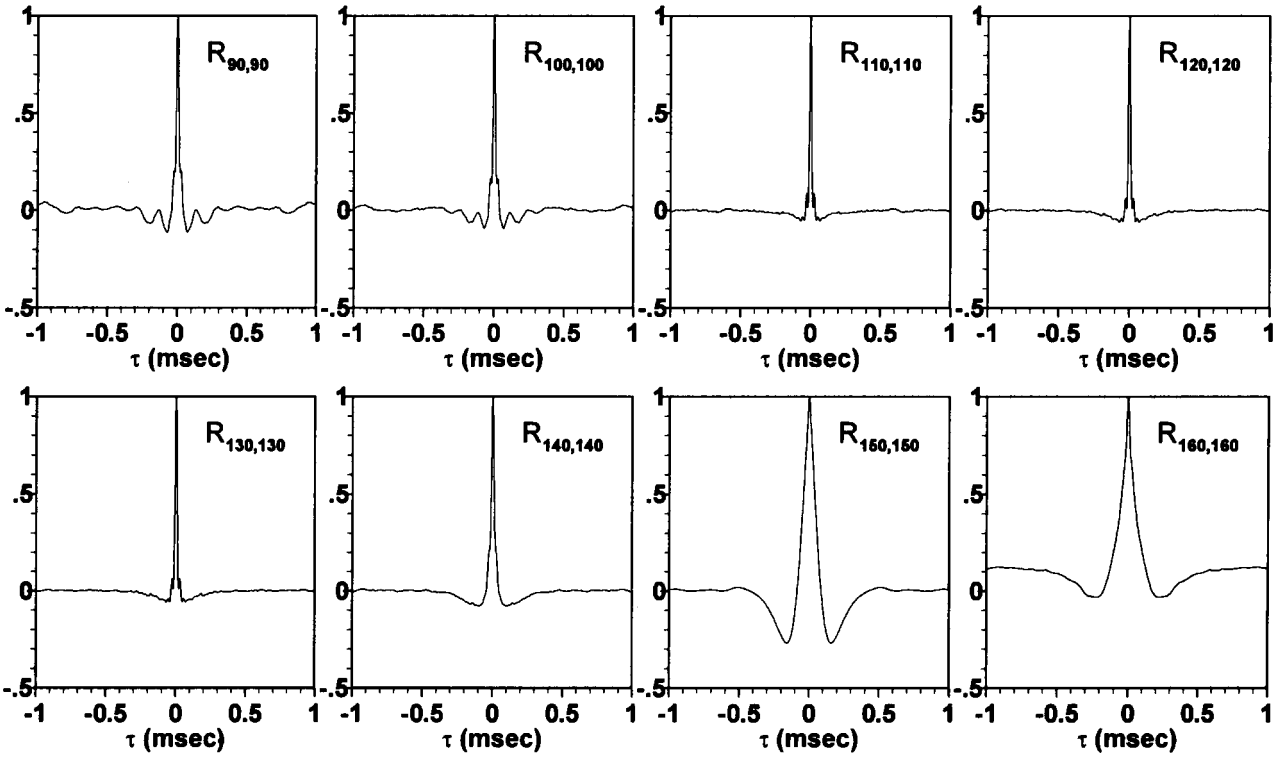

Fig.4 Auto-correlation for Microphones at all Locations (d) Rectangular Convergent Nozzle M=0.8, ϕ=90°

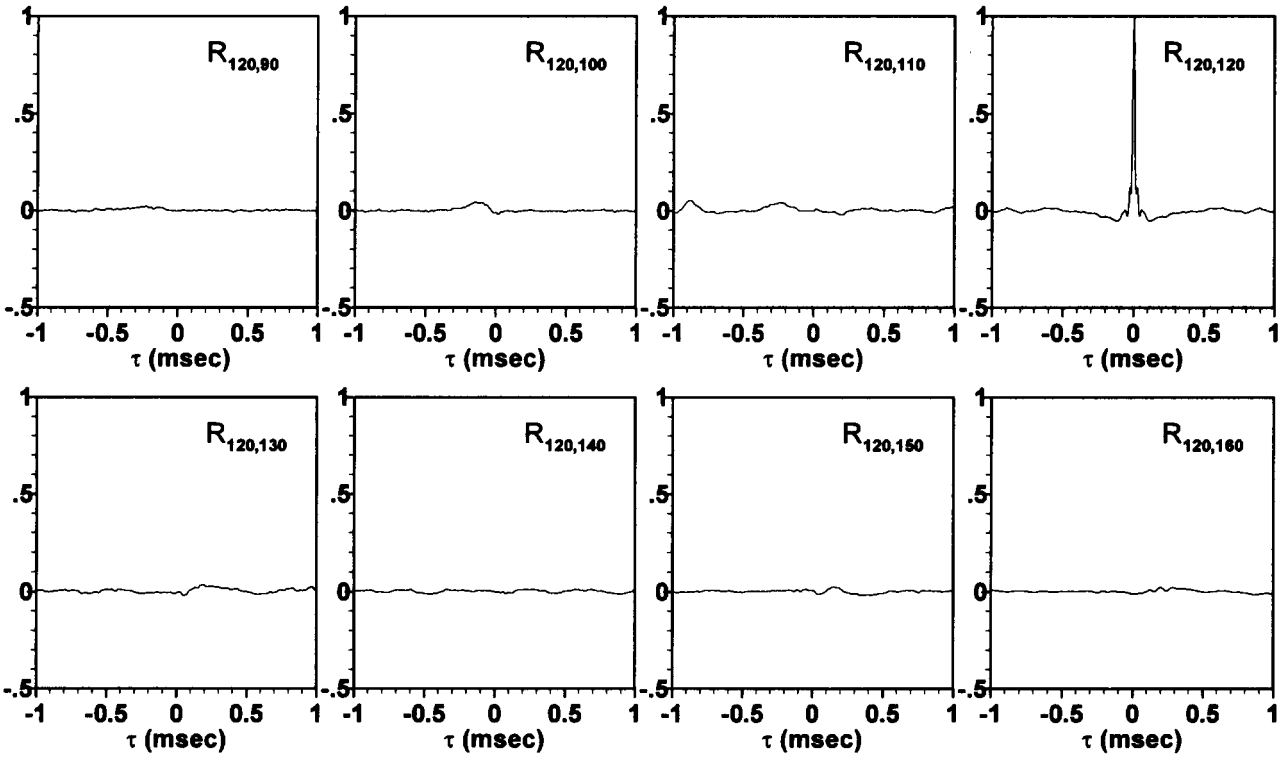

Fig.5 Cross Correlation at with Correlating Microphone at 120° (a) CD Nozzle M=1.5

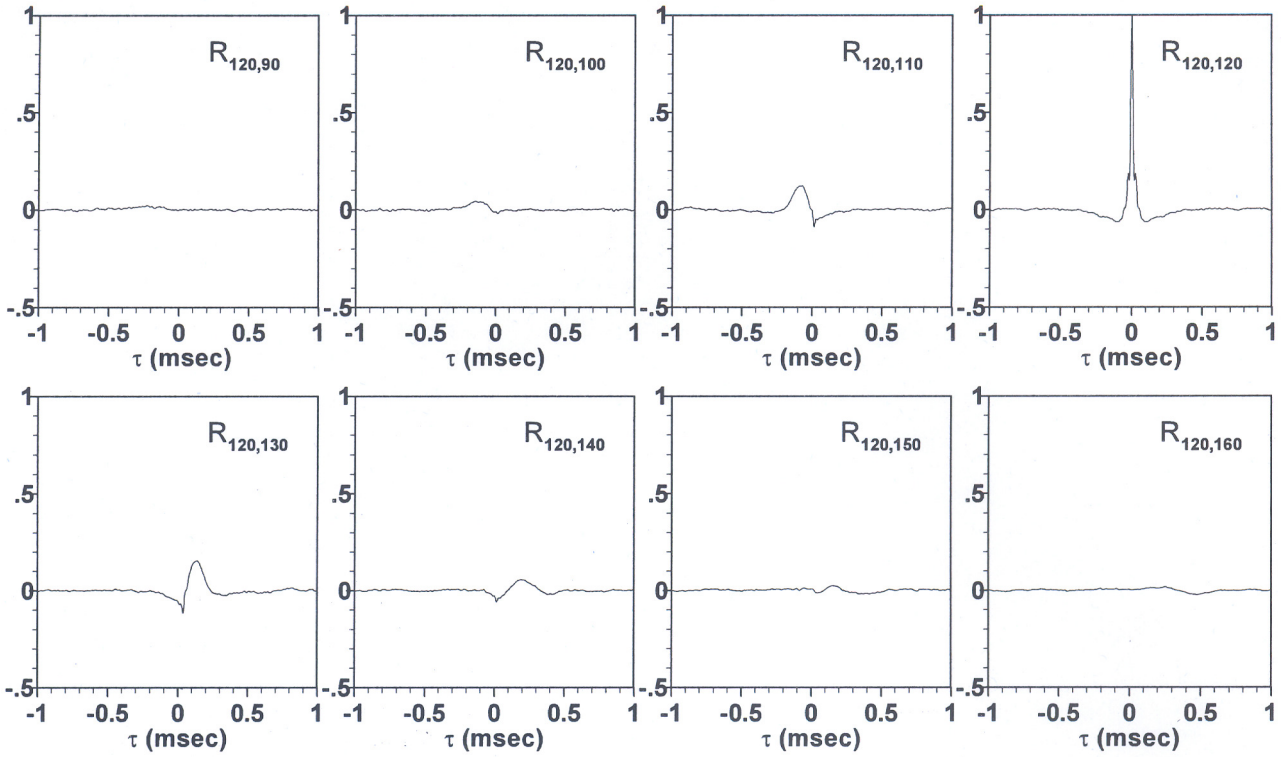

Fig.5 Cross Correlation at with Correlating Microphone at 120° (b) Circular Convergent Nozzle M=0.8

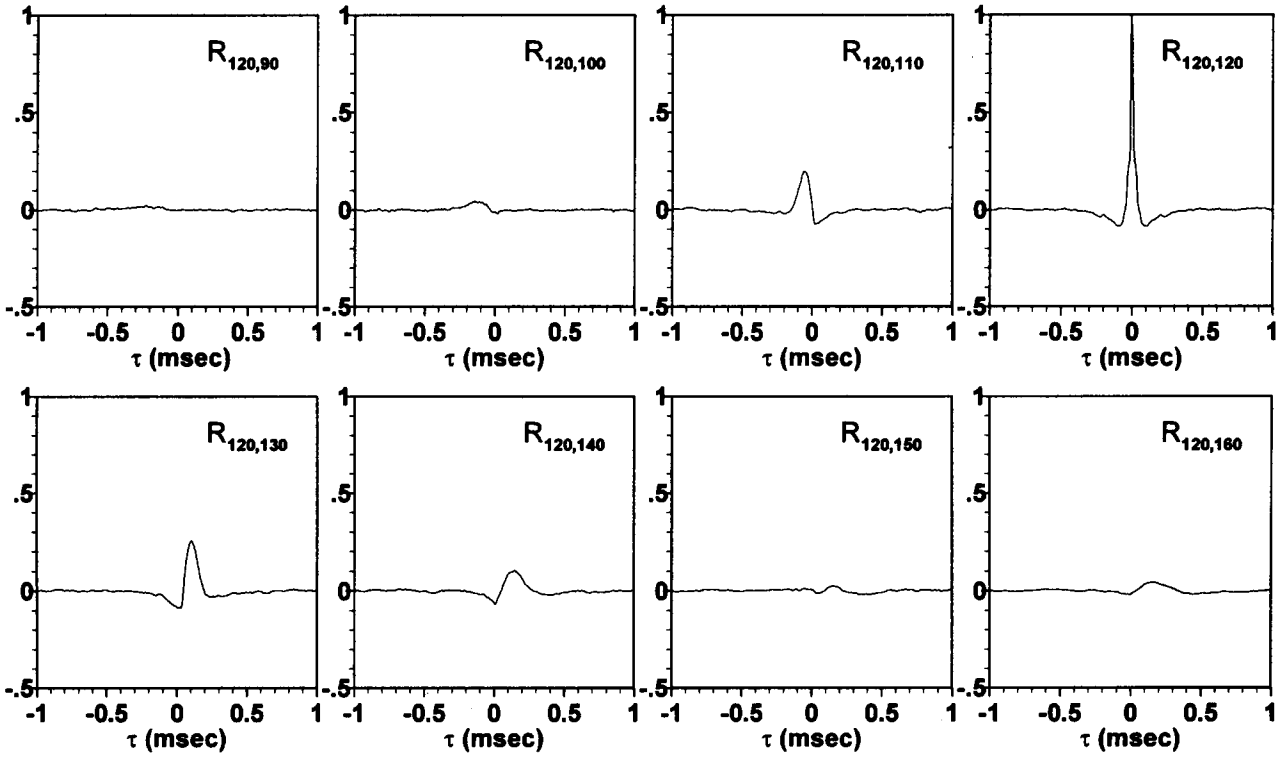

Fig.5 Cross Correlation at with Correlating Microphone at 120° (c) Rectangular Convergent Nozzle M=0.8, ϕ=0°

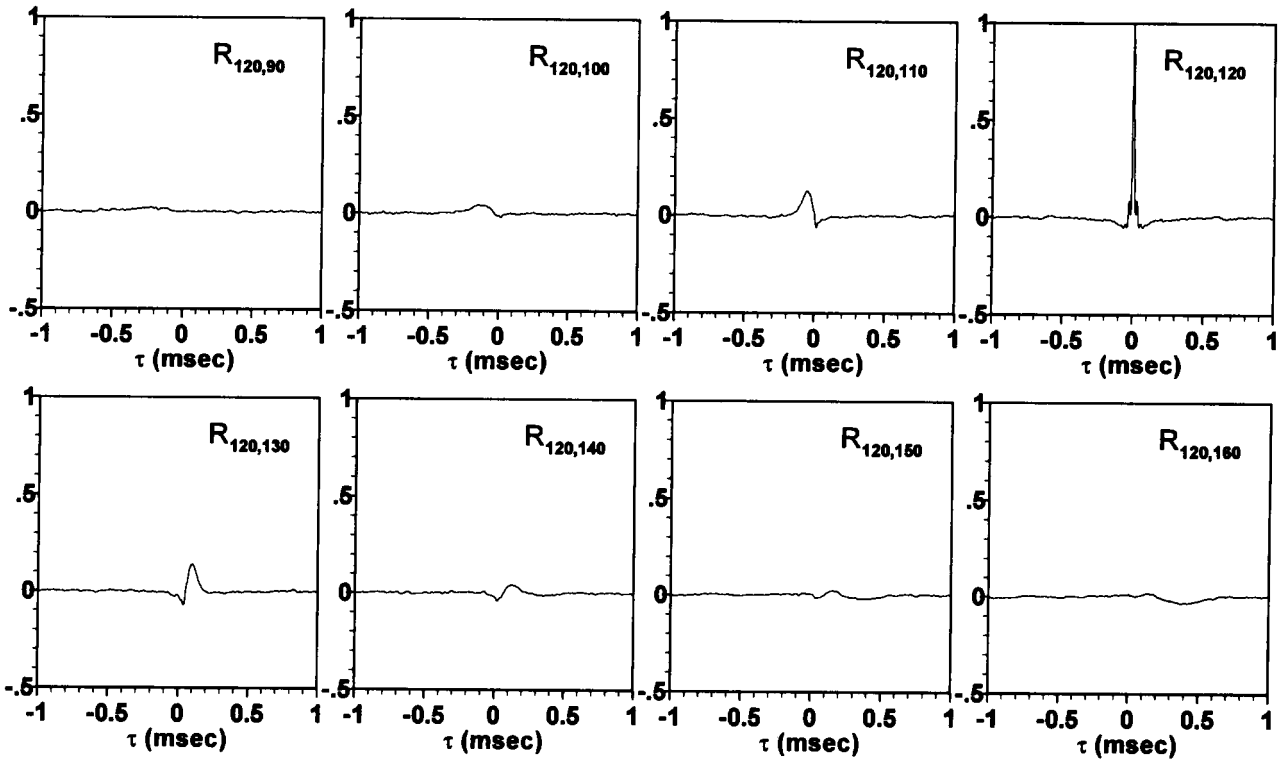

Fig.5 Cross Correlation at with Correlating Microphone at 120° (d) Rectangular Convergent Nozzle M=0.8, ϕ=90°

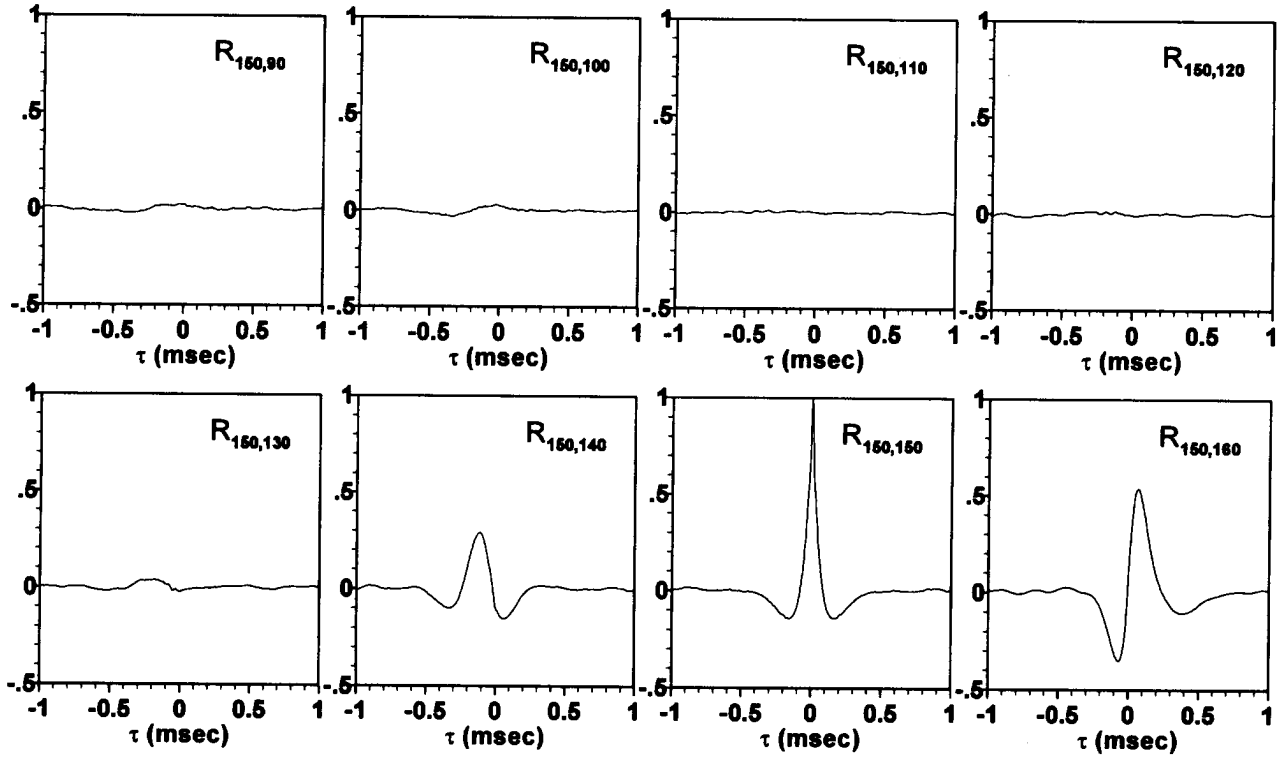

Fig.6 Cross Correlation with Correlating Microphone at 150° (a) CD Nozzle M=1.5

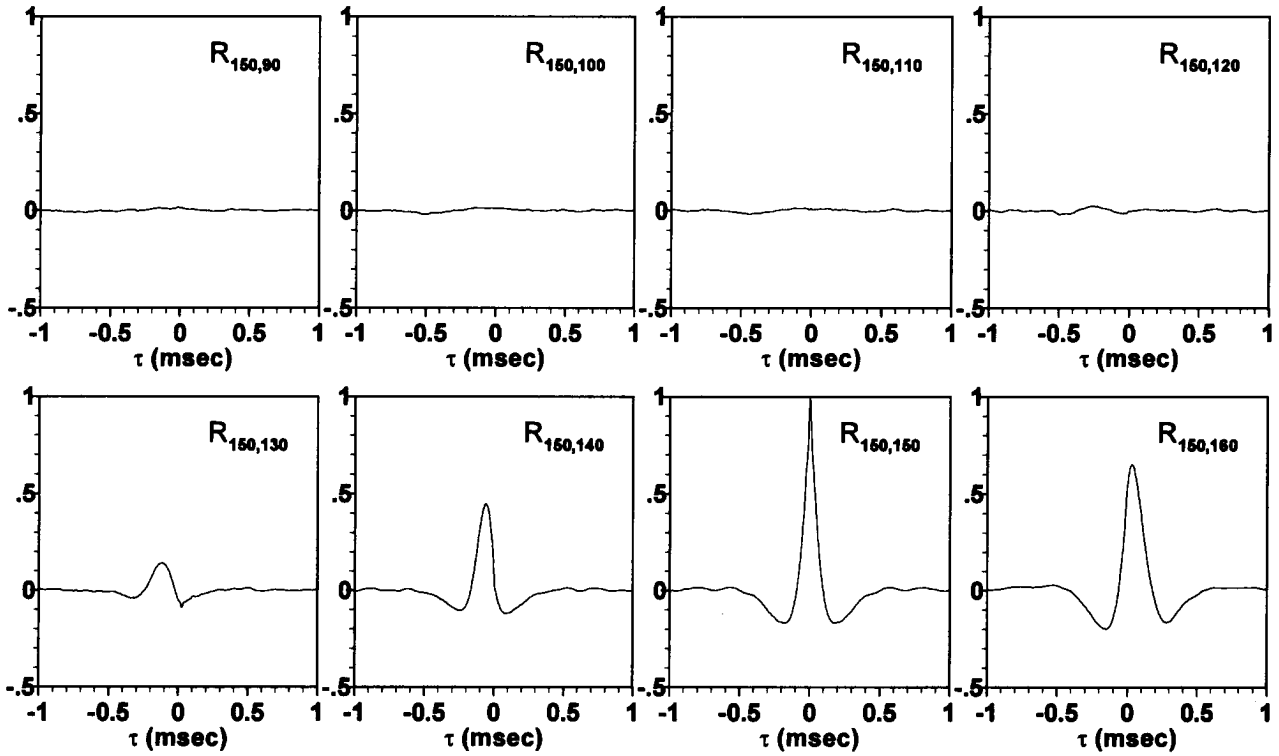

Fig.6 Cross Correlation with Correlating Microphone at 150° (b) Circular Convergent Nozzle M=0.8

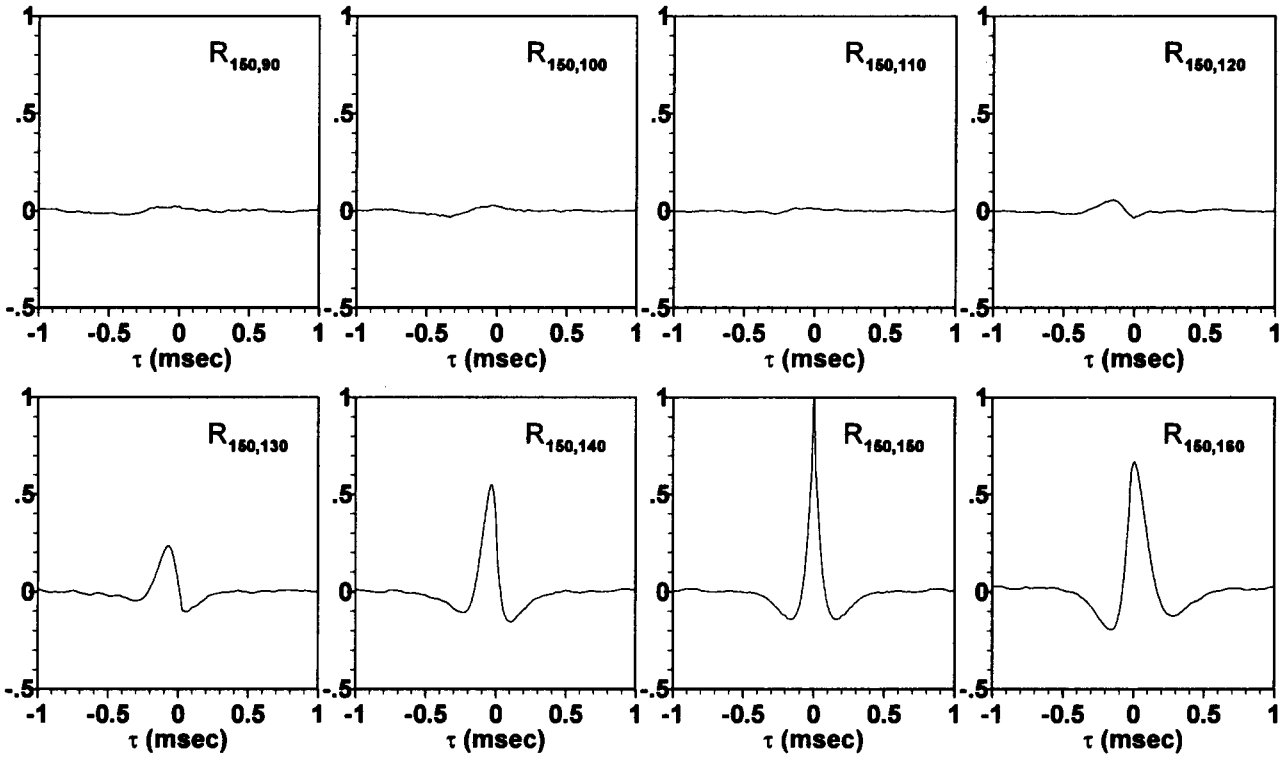

Fig.6 Cross Correlation with Correlating Microphone at 150° (c) Rectangular Convergent Nozzle M=0.8, ϕ=0°

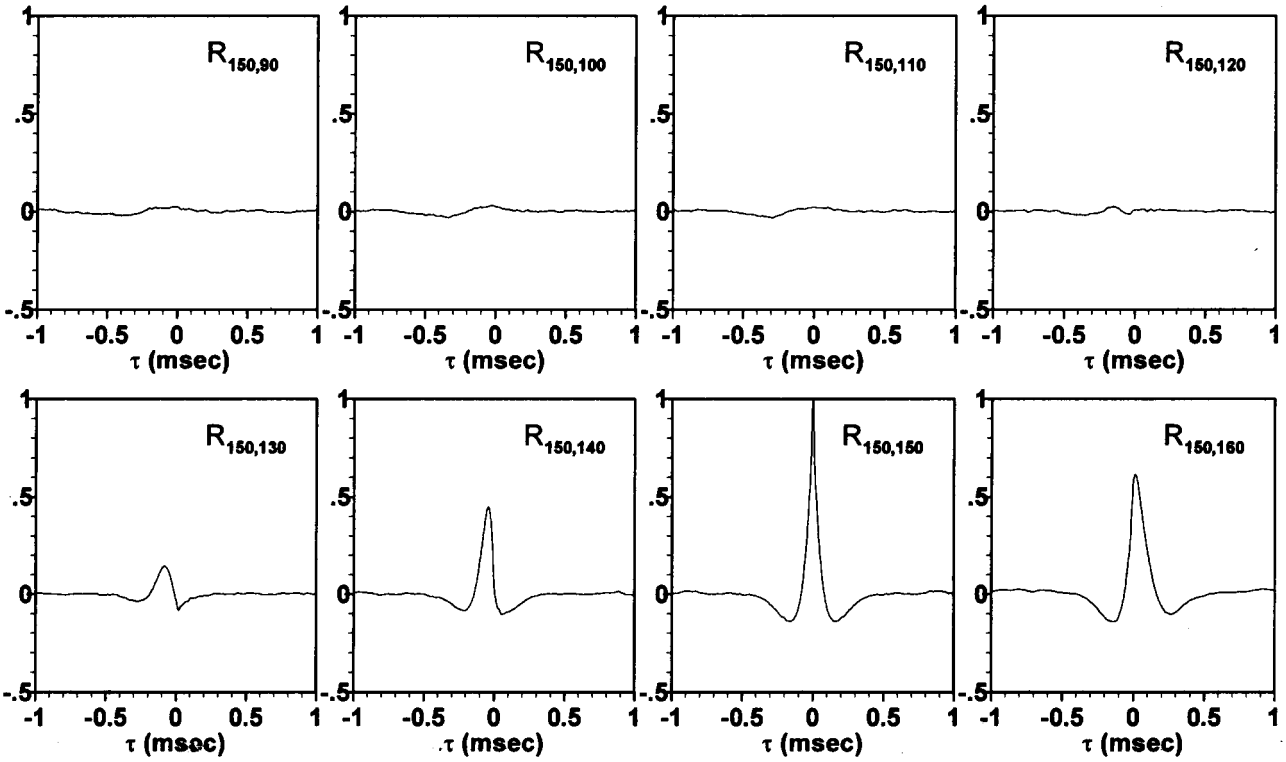

Fig.6 Cross Correlation with Correlating Microphone at 150° (d) Rectangular Convergent Nozzle M=0.8, ϕ=90°

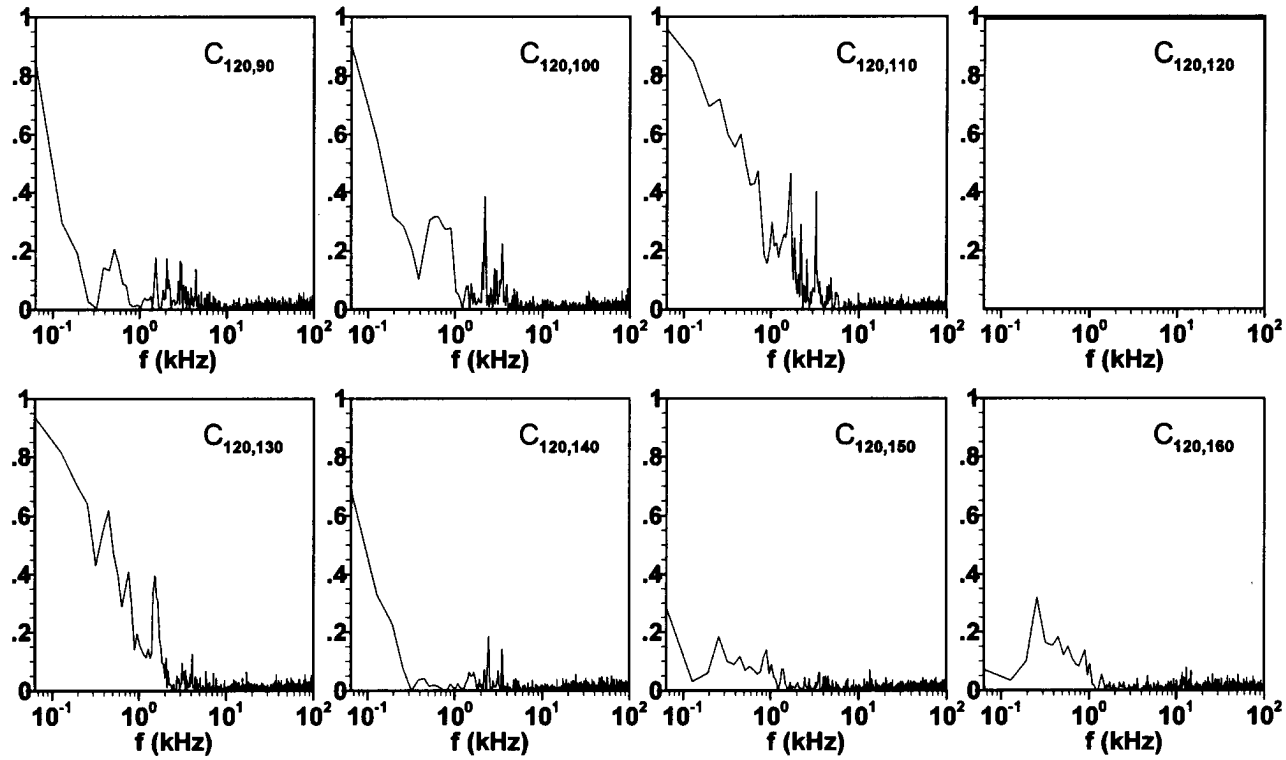

Fig.7 Coherence Function Values with Reference Microphone at 120° (a) CD Nozzle M=1.5

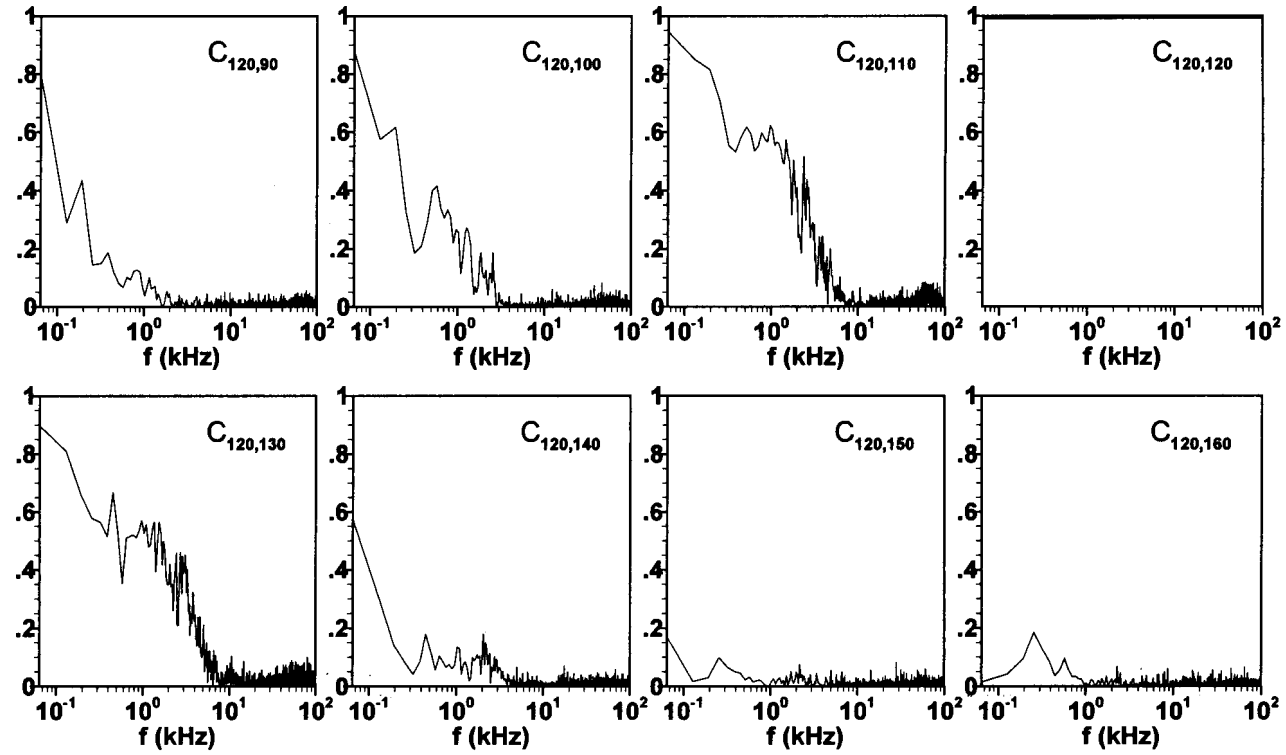

Fig.7 Coherence Function Values with Reference Microphone at 120° (b) Circular Convergent Nozzle M=0.8

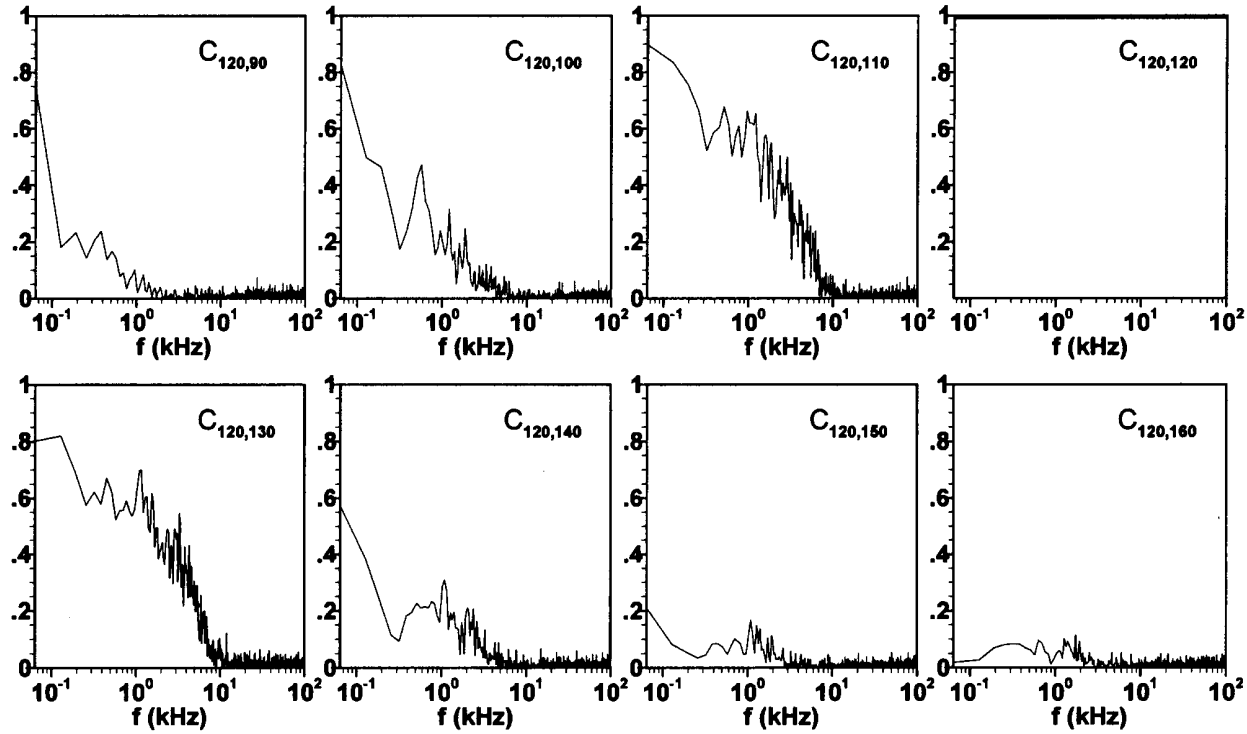

Fig.7 Coherence Function Values with Reference Microphone at 120° (c) Rectangular Convergent Nozzle M=0.8, ϕ=0°

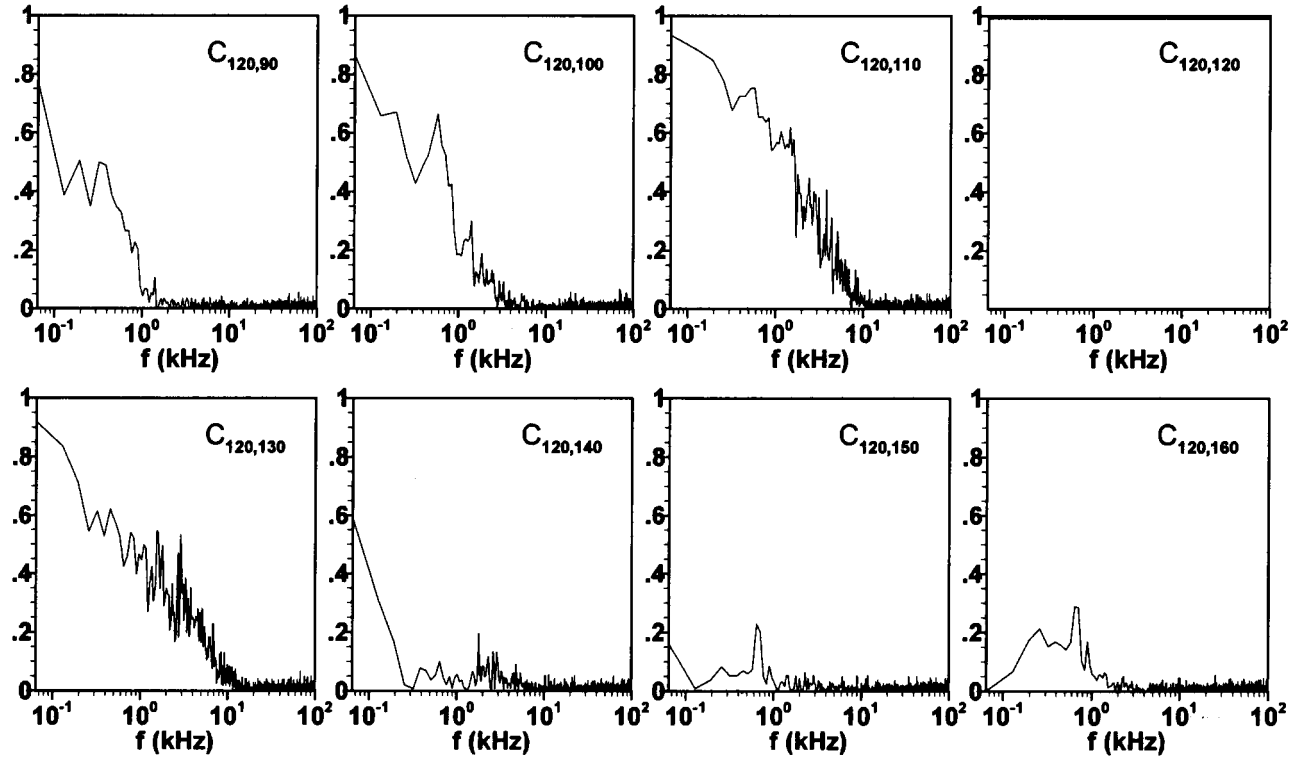

Fig.7 Coherence Function Values with Reference Microphone at 120° (d) Rectangular Convergent Nozzle M=0.8, ϕ=90°

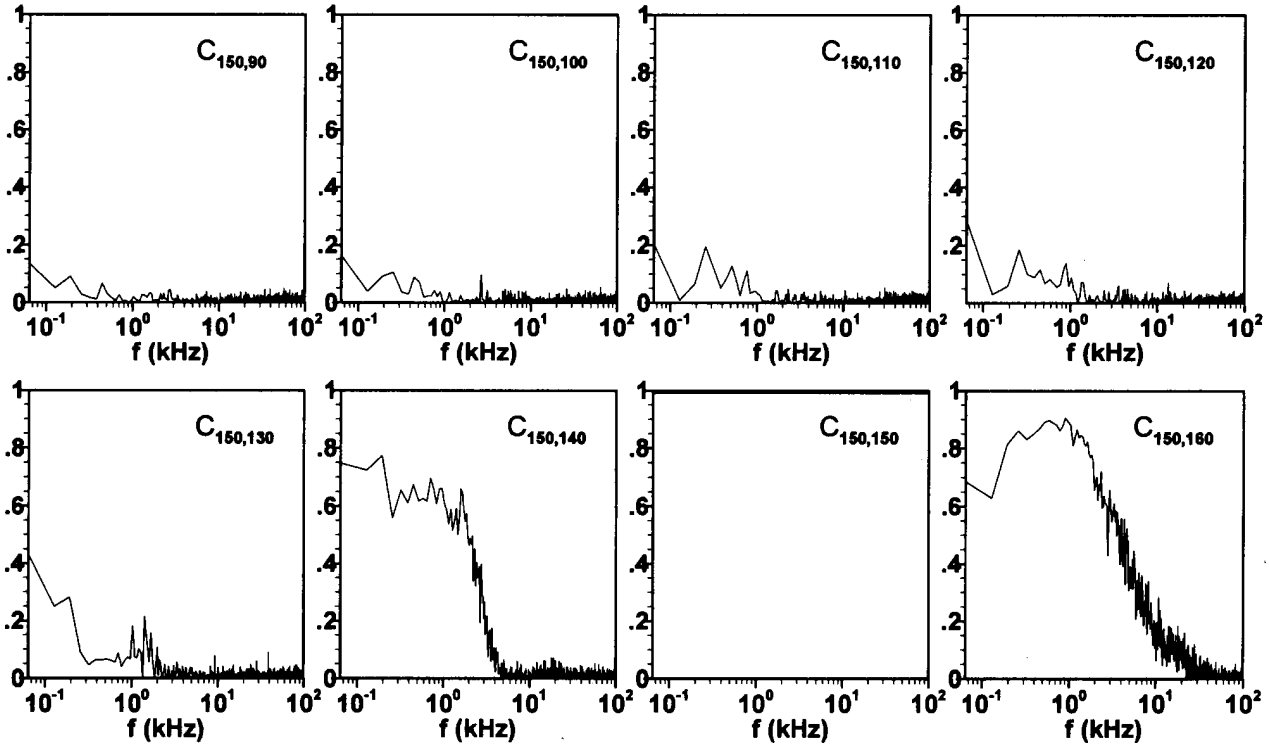

Fig.8 Coherence Function Values with Reference Microphone at 150° (a) CD Nozzle M=1.5

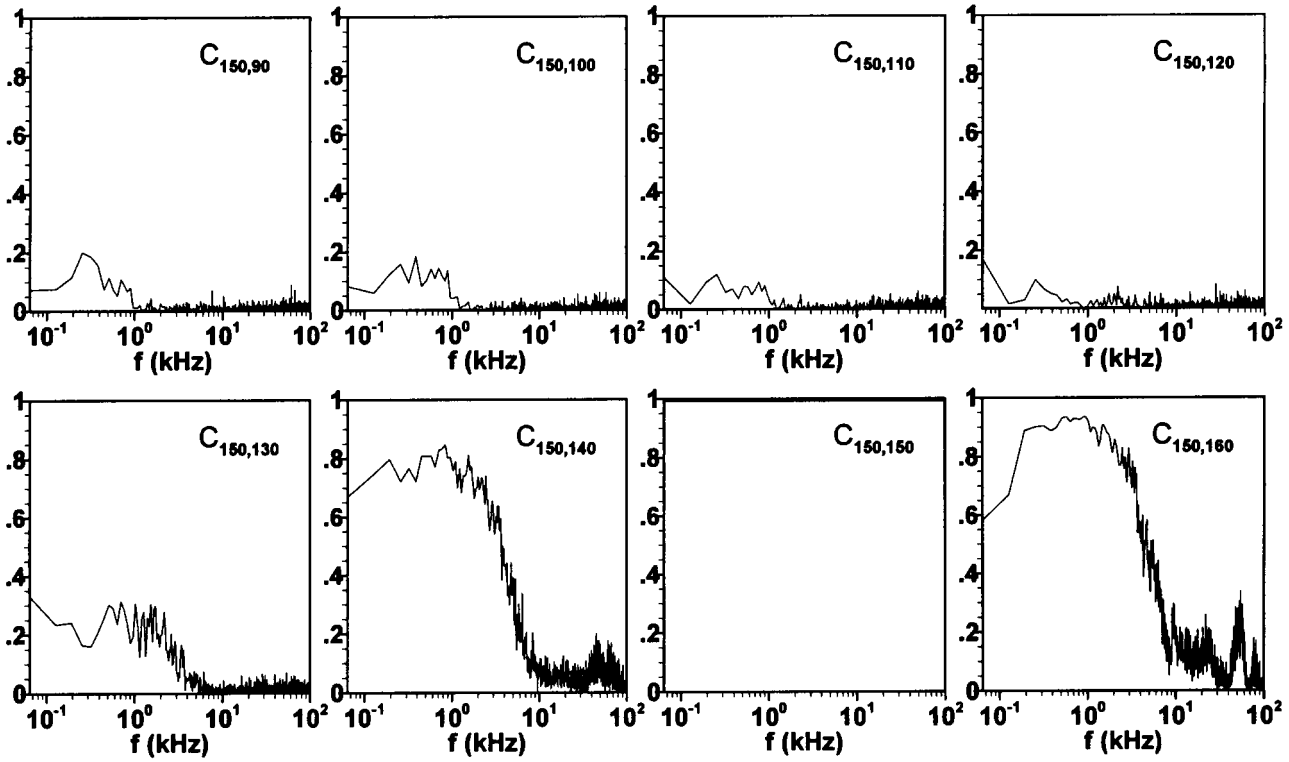

Fig.8 Coherence Function Values with Reference Microphone at 150° (b) Circular Convergent Nozzle M=0.8

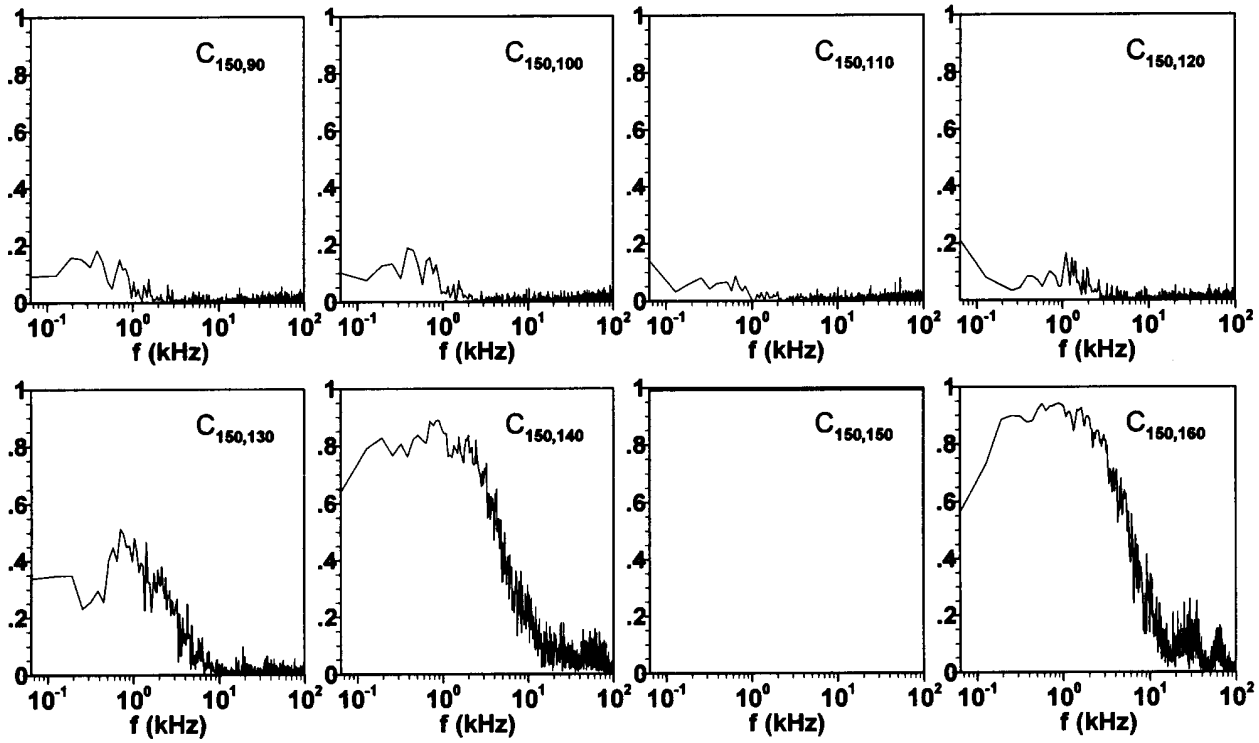

Fig.8 Coherence Function Values with Reference Microphone at 150° (c) Rectangular Convergent Nozzle M=0.8, ϕ=0°

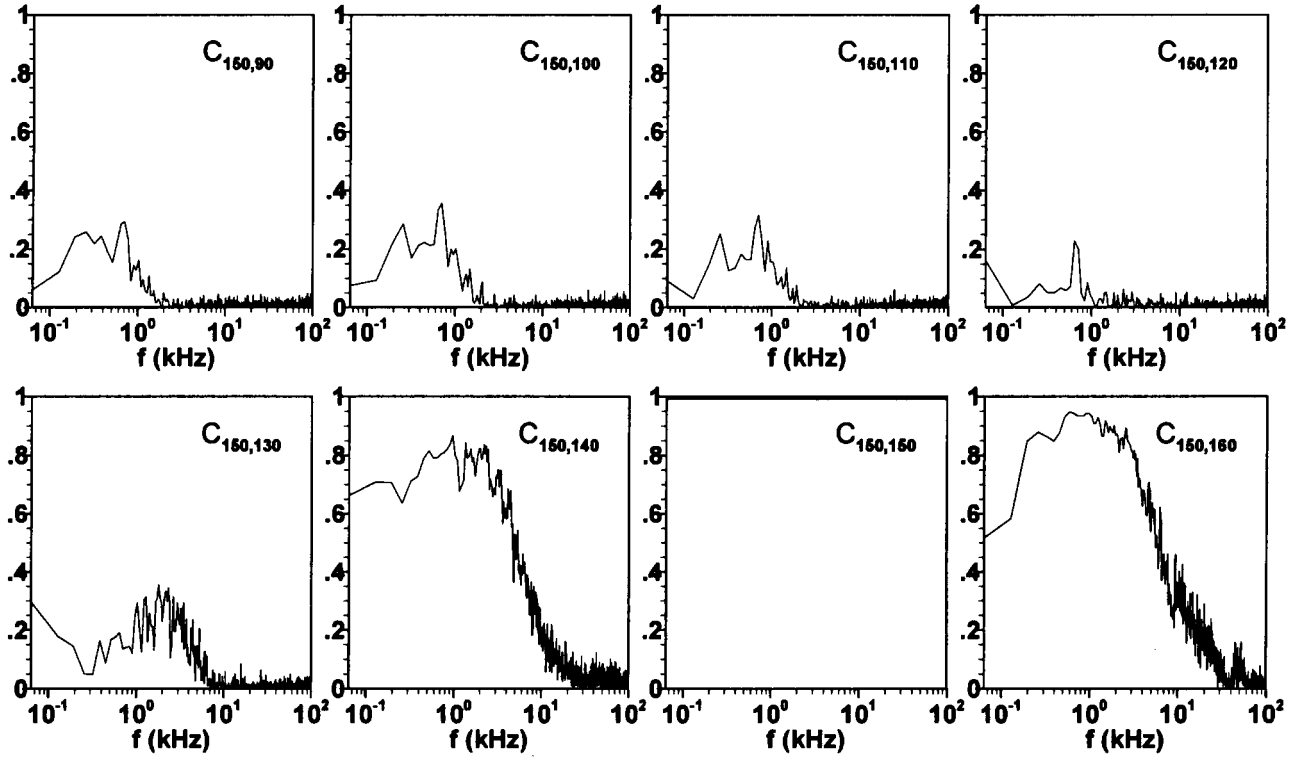

Fig.8 Coherence Function Values with Reference Microphone at 150° (d) Rectangular Convergent Nozzle M=0.8, ϕ=90°